Appendix A

PHOTOCHEMICAL OXIDATION OF NITRIC OXIDE SYNTHASE

A.1. Introduction to Nitric Oxide Synthases

Nitric oxide (NO) is a biological regulator and signaling molecule, and is involved in immune response of eukaryotes.[1,2] Biological NO production is catalyzed by Nitric Oxide Synthase (NOS), a heme monooxygenase that shares the thiolate-ligation motif with chloroperoxidase and cytochrome P450. Three isoforms of NOS exist in mammals, including endothelial, inducible, and neuronal NOS. All three isoforms exist as homodimers, and are composed of two domains (**Figure A.1**).[3] The oxygenase domain contains the thiolate-ligated heme and the redox cofactor tetrahydrobiopterin (THB or H_4B). The calmodulin-linked reductase domain contains the flavin cofactors flavin adenine dinucleotide (FAD) and flavin mononucleotide (FMN); this domain is responsible for delivering electrons to the heme.

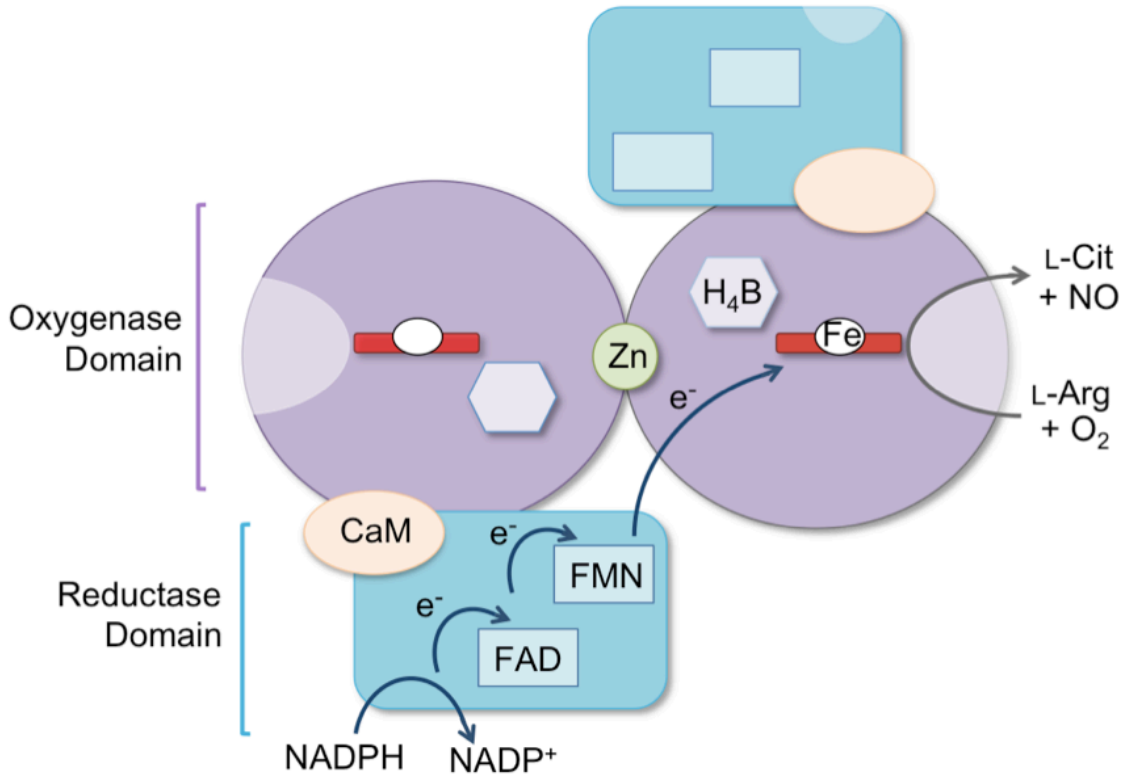

Figure A.1. Cartoon of the NOS homodimeric structure, highlighting pathways for electron flow (reproduced from ref. 10, Thesis by G. E. Keller).

Recently, NOS-like enzymes have also been found in bacteria (**Figure A.2**).[4,5] These enzymes have strong structural and sequence similarities to their mammalian counterparts, though many are composed solely of the oxygenase domain (and lack the reductase domain).[6] Bacterial NOS enzymes have been shown to produce NO *in vitro* and *in vivo,*[6] and can be used as more stable homologues in which to study aspects of NOS catalysis.

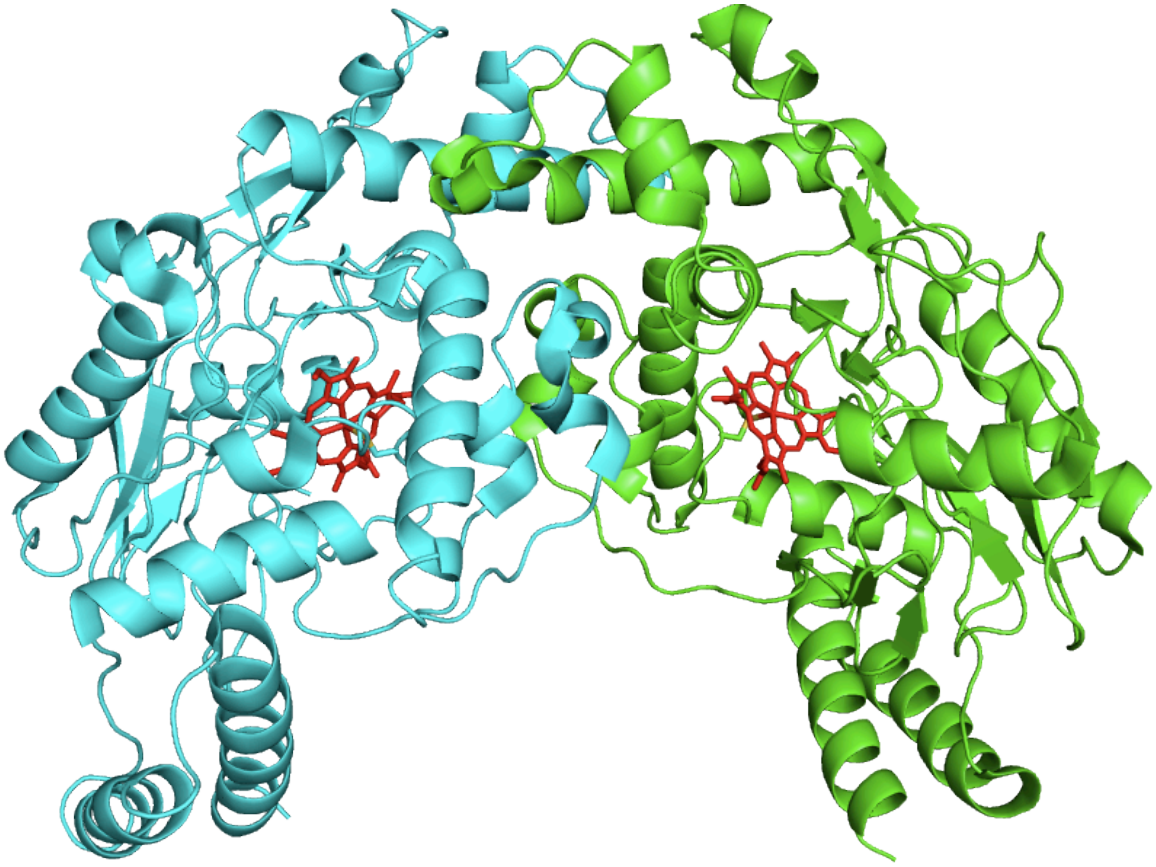

Figure A.2. Dimeric structure of NOS from *Geobacillus stearothermophilus*. PDB: 2FLQ.

NOS catalyzes the production of NO in two turnovers from L-arginine, releasing L-citruline as a biproduct (**Figure A.3**). Many aspects of the catalytic cycle have yet to be determined for NOS, including the identity of the catalytically active species. However, the first turnover is believed to be similar to P450 catalysis, involving

production of a ferryl-ligand radical cation species known as compound I (CI) (**Figure A.4**, blue arrows).

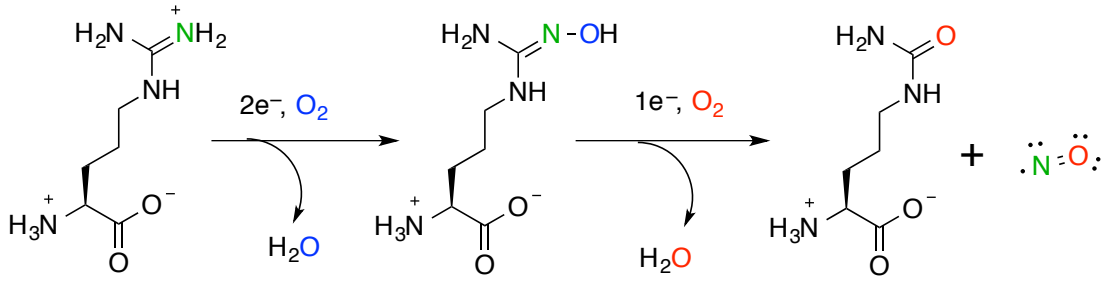

Figure A.3. NOS-catalyzed production of nitric oxide from L-arginine.

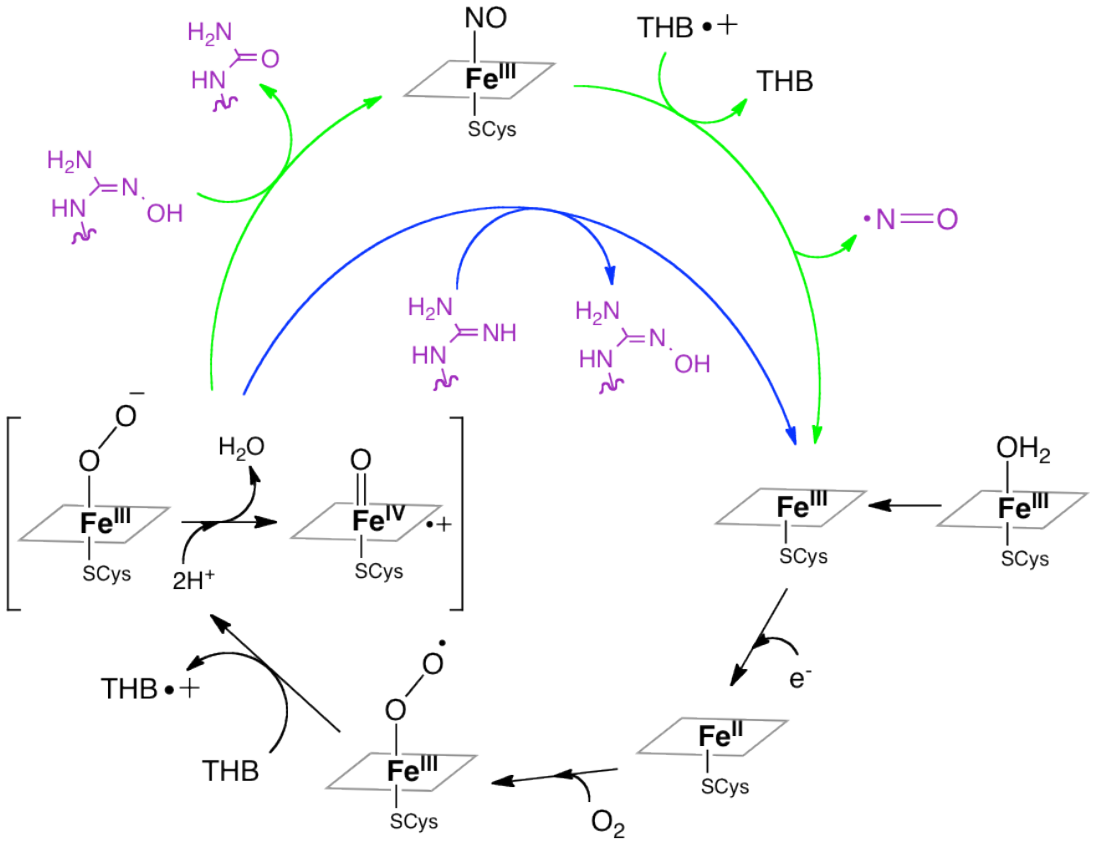

Figure A.4. Proposed catalytic cycle for NOS. Blue arrows indicate the first turnover, green arrows indicate the second turnover. Possible catalytically active species are in brackets.

In both turnovers, two reductive electron transfers (ET) steps activate molecular oxygen (**Figure A.4**, black arrows). In contrast to cytochrome P450, in which both

electrons are relayed to the heme via flavin cofactors from a reductase domain, the second electron in NOS catalysis is delivered from the bound THB cofactor. The active species (proposed to be CI) hydroxylates the guanidinyl nitrogen of L-arginine, producing N-hydroxy-L-arginine as a stable, bound intermediate, and regenerating the resting (ferric) form of the enzyme. The second turnover, which produce NO, is an odd-electron process that is unique in biology.[7] Again, an equivalent of molecular oxygen is activated, to form either a CI or ferric-peroxo active species (**Figure A.4**, in brackets). N-hydroxy-L-arginine is oxidized to produce L-citrulline and release nitric oxide. Full NO production requires THB; in the absence of this cofactor, nitrite and cyano-ornithine are produced rather than nitric oxide and citrulline.[8]

As described in Chapters 2-5, we developed photosensitizer-P450 conjugates that replace native ET partners with ruthenium diimine complexes that are bound to the P450 surface at a non-native cysteine. Laser-triggered flash-quench methods (**Figure A.5,** described in Chapter 1) allowed rapid oxidation or reduction of the P450 heme, on the microsecond timescale.

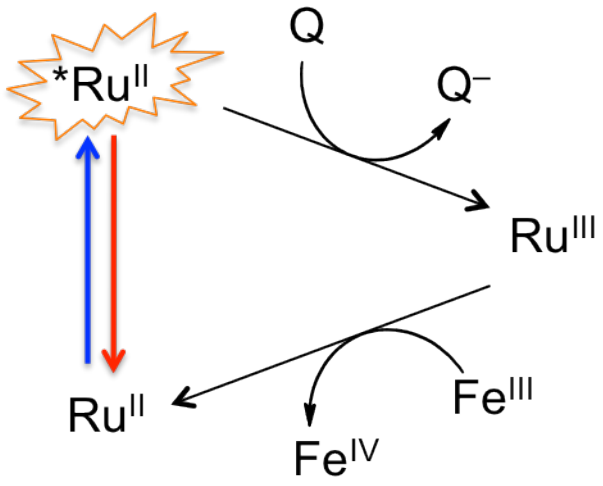

Figure A.5. Flash-quench cycle for oxidizing the heme active site (Fe).

Inspired by the proposed similarities, and intriguing differences, between NOS and P450 catalytic cycles, we set out to determine whether similar flash-quench of Ru-NOS conjugates could be used to probe NOS catalysis. In particular, we were interested in investigating the thermophilic bacterial NOS from *Geobacillus stearothermophilus* (gsNOS), which has been examined by other members of the Gray group.[9,10] This Appendix describes the development and photophysical characterization of Ru-NOS conjugates, and analysis of photochemical NOS oxidation using time-resolved transient absorption (TA) studies.

A.2. Results

A.2.1. Ru-photosensitizer conjugation

Selection of NOS mutant and Ru photosensitizer

Analogous to the Ru-P450 systems, cysteine-specific labeling was chosen to covalently tether the ruthenium photosensitizer. A mutant enzyme containing a single surface-exposed cysteine was designed by Dr. Charlotte Whited (**Figure A.6**). Two native, surface-exposed cysteines have been removed by mutagenesis: C227S/C269S, and a single cysteine installed: K115C. The exposed cysteine (K115C) is distant from the dimer interface, and it was anticipated that Ru-labeling at this site would not perturb dimer formation.

We have labeled K115C gs NOS with the photosensitizer [Ru(2,2′-bipyridine)$_2$(5-iodoacetamido-1,10-phenanthroline)]$^{2+}$ (abbreviated [Ru(bpy)$_2$(IAphen)]$^{2+}$), in analogy to studies with cytochrome P450. Ru-NOS conjugation is achieved in high yield within 4 hours at 4 °C.

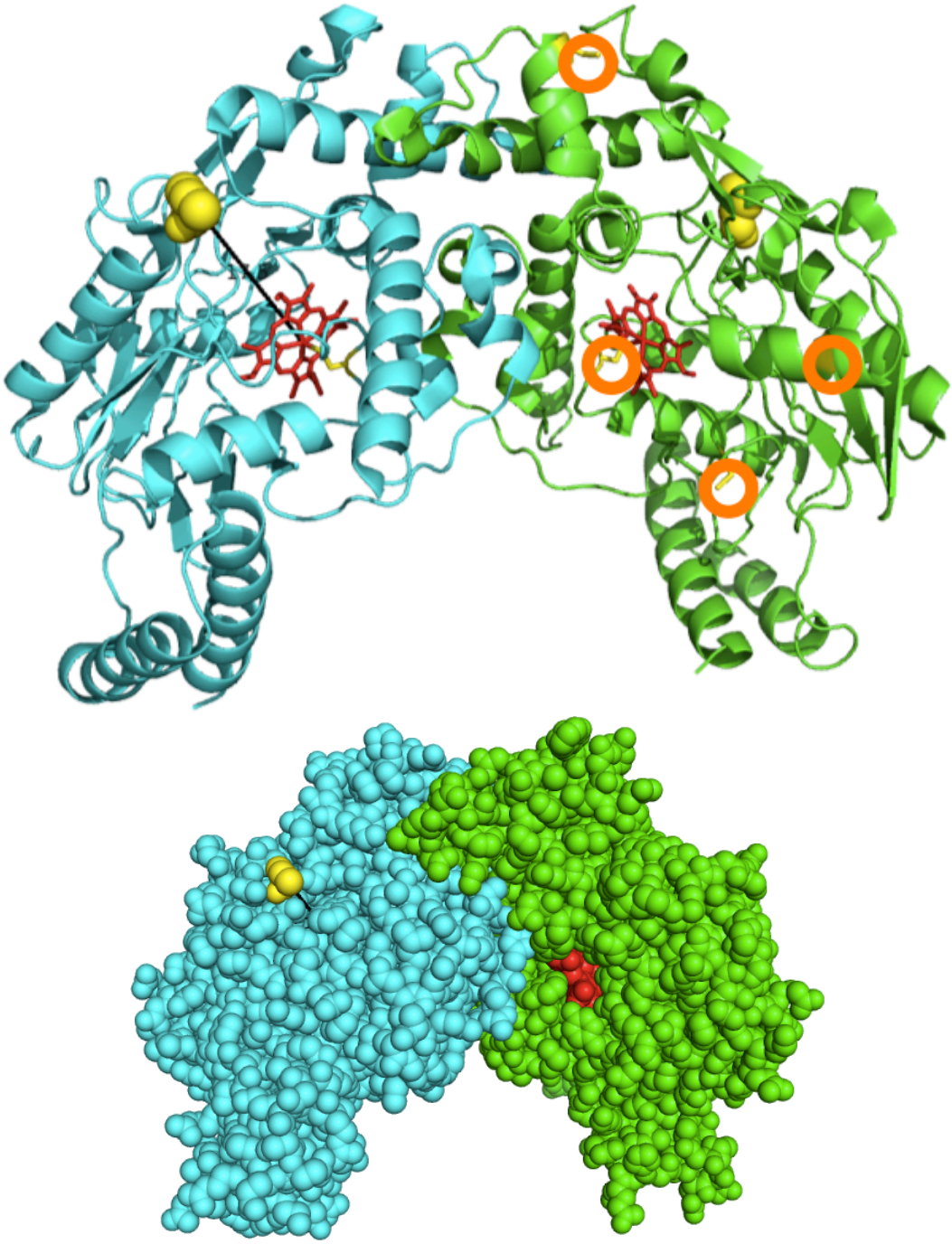

Figure A.6. Location of the photosensitizer tethering site. The NOS heme is colored red, K115C is highlighted in yellow. **Top**: Four native cysteines (including the one that ligates the heme) are circled in orange. **Bottom**: Space filling model, showing surface exposure of K115C, away from the dimer interface.

Characterization of Ru-NOS

The Ru-NOS conjugate has been characterized by mass spectrometry and UV-visible absorption (**Figure A.7**). The mass of Ru-NOS (MW = 44,516 Da) corresponds to that of apo (heme-free) K115C NOS (MW = 43866) plus the mass of the photosensitizer minus the mass of iodide (MW = 652 Da). In addition to typical NOS Soret and Q-bands, the absorption spectrum of Ru-NOS clearly shows a shoulder at 450 nm, which is attributed to photosensitizer absorbance. The crystal structure of this conjugate, Ru_{C115}-NOS, has been obtained by the Crane laboratory in collaboration with Dr. Gretchen Keller (**Figure A.8**).[10]

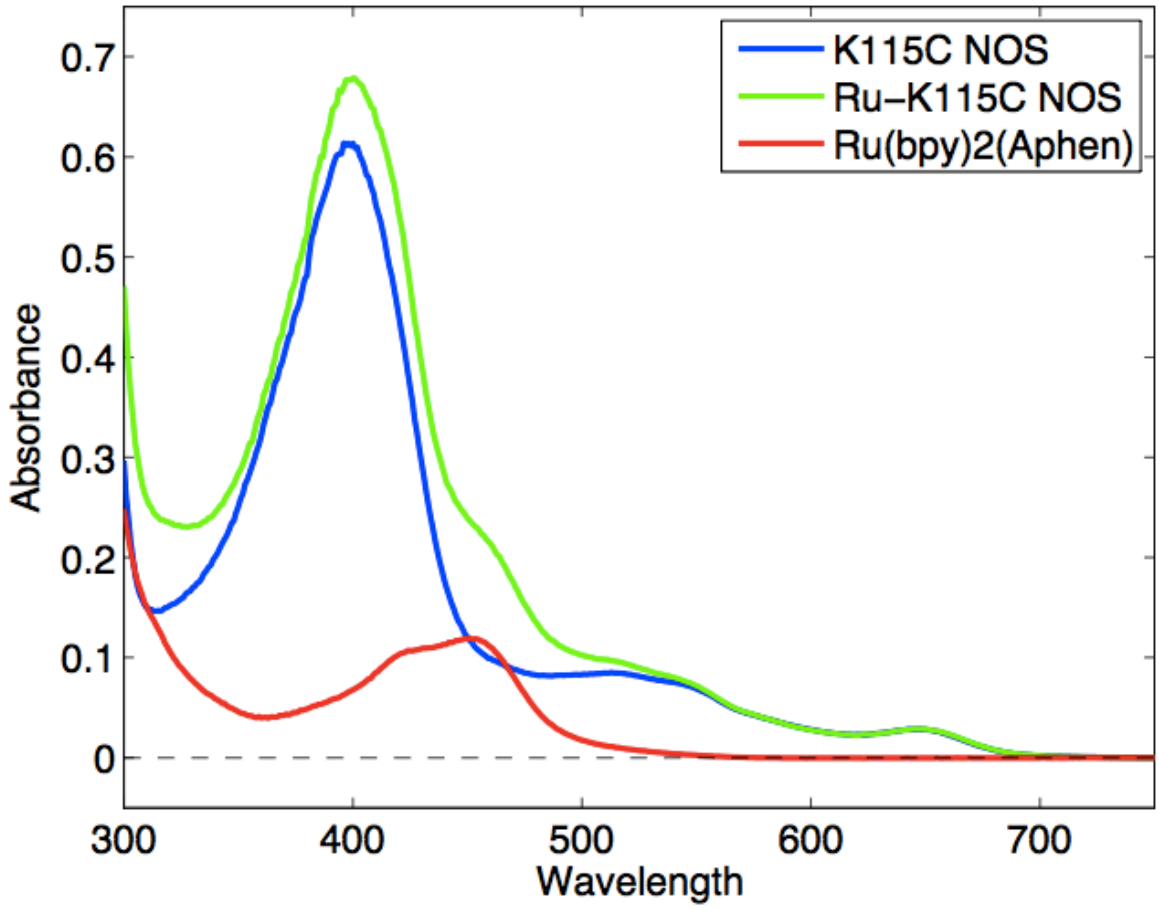

Figure A.7. UV-visible absorption of unlabeled and labeled Ru-NOS and free photosensitizer.

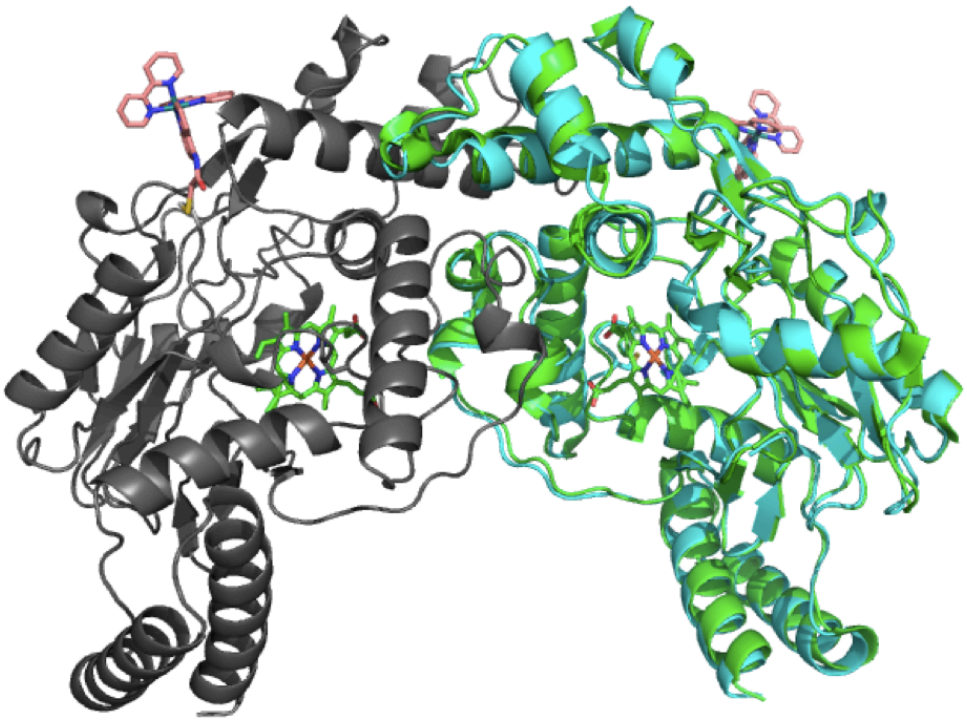

Figure A.8. Structure of Ru-NOS. The Ru-NOS dimer is shown in gray and cyan; the latter monomer is overlayed with wild-type NOS (green, PDB 2FLQ). The tethered Ru complex is colored pink. Figure reproduced from ref 10, G. E. Keller.

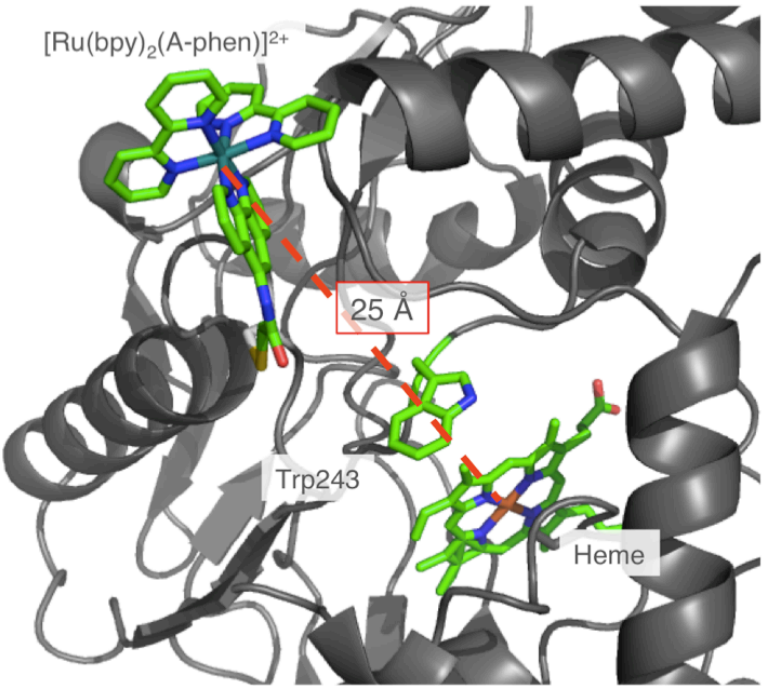

Figure A.9. Tryptophan 243 is located between the photosensitizer and heme in Ru-NOS. The Ru-Fe distance is 25 Å. Figure reproduced from ref 10, G.E. Keller.

A.2.2. Ru-NOS Luminescence

All time-resolved experiments are performed using deoxygenated samples (see sample preparation in Materials and Methods).

As described in Chapters 2, the free $[Ru(bpy)_2(Aphen)]^{2+}$ photosensitizer is emissive (λ_{max}=620 nm) when excited with blue light (e.g., 480 nm). The time-resolved luminescence decay of this complex in deoxygenated water can be fit to a monoexponential decay with a lifetime of 720 ns. In contrast, the time-resolved luminescence decay of Ru-NOS is clearly biexponential (**Figure A.10**). In deoxygenated buffer (50 mM sodium borate, pH 8), the major decay component (~75%) has a decay constant τ_A = 150 ns, while the minor component (~25%) is significantly longer, with τ_B = 1100 ns. Bi-exponential luminescence decay also was observed for Ru-P450 conjugates (see Chapters 2 and 3), and was attributed to multiple conformations of the photosensitizer that do not exchange on the timescale of luminescence decay.

Given the dimeric nature of NOS in solution,[9] we were interested to investigate whether this biexponential luminescence was related to a monomer-dimer equilibrium. The ratio of major and minor decay components is invariant over a Ru-NOS concentration range of 1-20 μM (**Table A.1**). This ratio and concentration-independence is identical at high ionic strength (500 mM sodium chloride) (**Table A.2**). Interestingly, the luminescence decay rate of the major component is affected by ionic strength, while the minor component is not (**Figure A.11**).

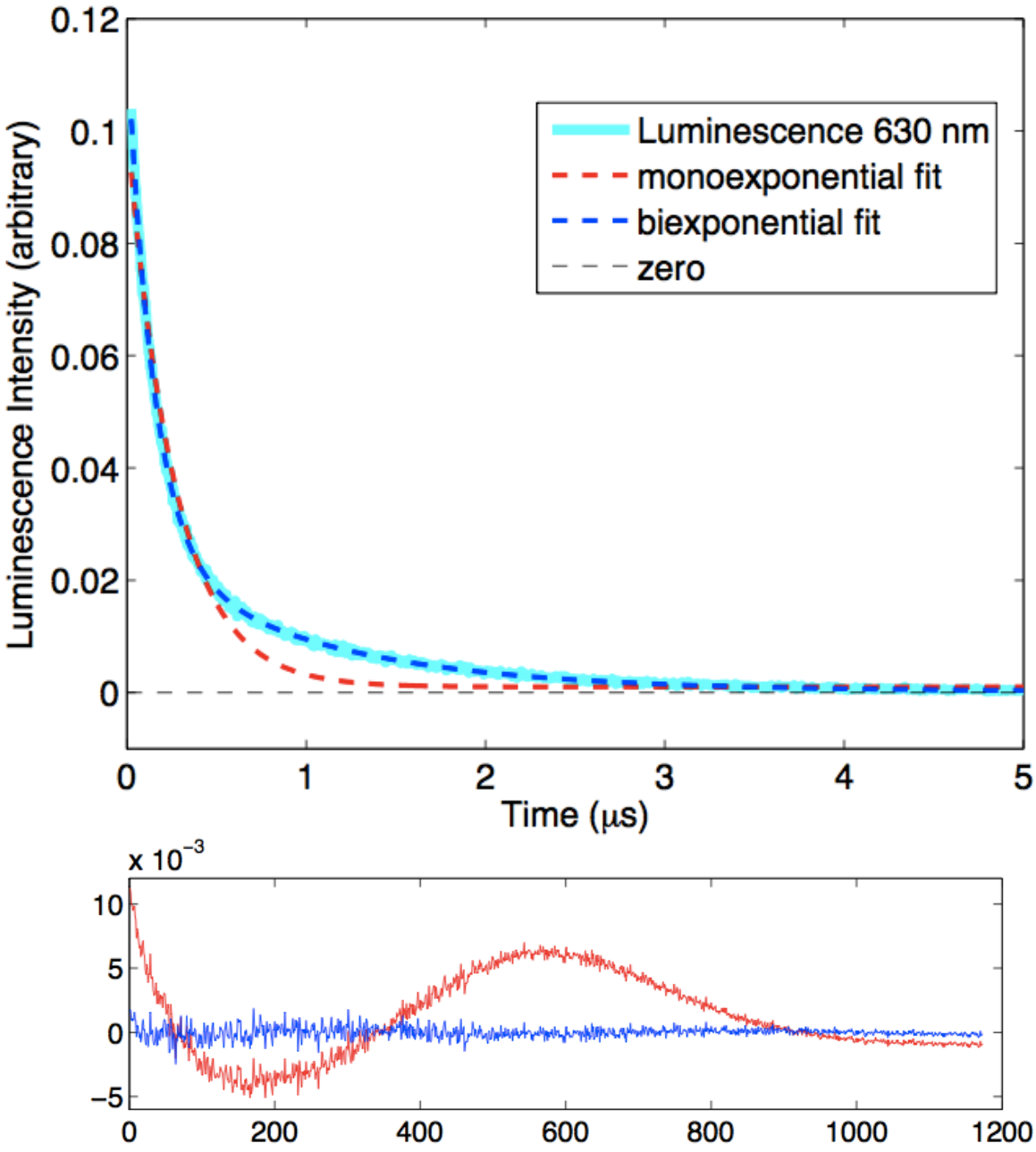

Figure A.10. Top: Luminescence decay of Ru-K115C NOS, fit to a single (red) and double (blue) exponential function. **Bottom**: Residuals from mono- (red) and bi- (blue) exponential fits.

Table A.1. Luminescence lifetimes of Ru-NOS in 50 mM borate buffer, pH 8. A and B are the major and minor components of biexponential decay, respectively.

Conc (μ M)	A: τ (ns) / %	B: τ (ns) / %
1	155 / 77%	1098 / 23%
3	149 / 76%	1042 / 24%
6	154 / 76%	1136 / 24%
9	154 / 76%	1120 / 24%
14	156 / 76%	1151 / 24%
20	155 / 76%	1148 / 24%

Table A.2. Luminescence lifetimes of Ru-NOS in 500 mM sodium chloride, 50 mM borate buffer, pH 8. A and B are the major and minor components of biexponential decay, respectively.

Conc (μ M)	A: τ (ns) / %	B: τ (ns) / %
1	106 / 76%	968 / 24%
3	107 / 75%	962 / 25%
6	107 / 76%	957 / 24%
9	107 / 75%	951 / 25%
13	108 / 76%	965 / 24%
20	111 / 75%	1014 / 25%

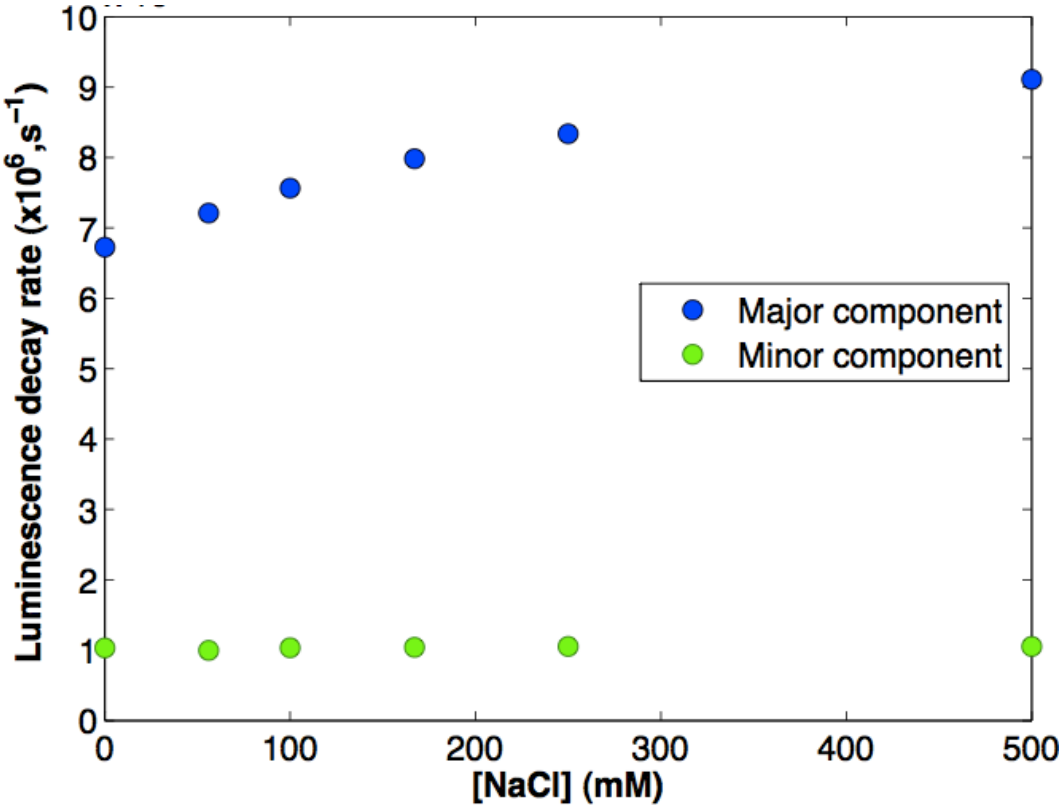

Figure A.11. Luminescence lifetimes of Ru-NOS at varying ionic strengths. Major (blue) and minor (green) decay components are plotted with respect to concentration of sodium chloride.

Luminescence quenching with $[Ru^{III}(NH_3)_6]^{3+}$

We also examined ET quenching of the Ru-NOS excited state by $[Ru^{III}(NH_3)_6]^{3+}$. As observed for P450, addition of $[Ru^{III}(NH_3)_6]^{3+}$ causes protein precipitation in buffers of low ionic strength; this occurs for both Ru-labeled and unlabeled NOS samples. Little or no precipitation is observed for protein samples in buffers of high ionic strength (~200 mM sodium chloride). All quenching experiments are performed in buffers with 250 mM sodium chloride, in addition to 50 mM sodium borate, pH 8.

Interestingly, the major component is significantly more affected by $[Ru^{III}(NH_3)_6]^{3+}$ concentration than the minor component (**Figure A.12**).

Additionally, the ratio of major-to-minor decay components increases at high quencher concentration (**Figure A.13**).

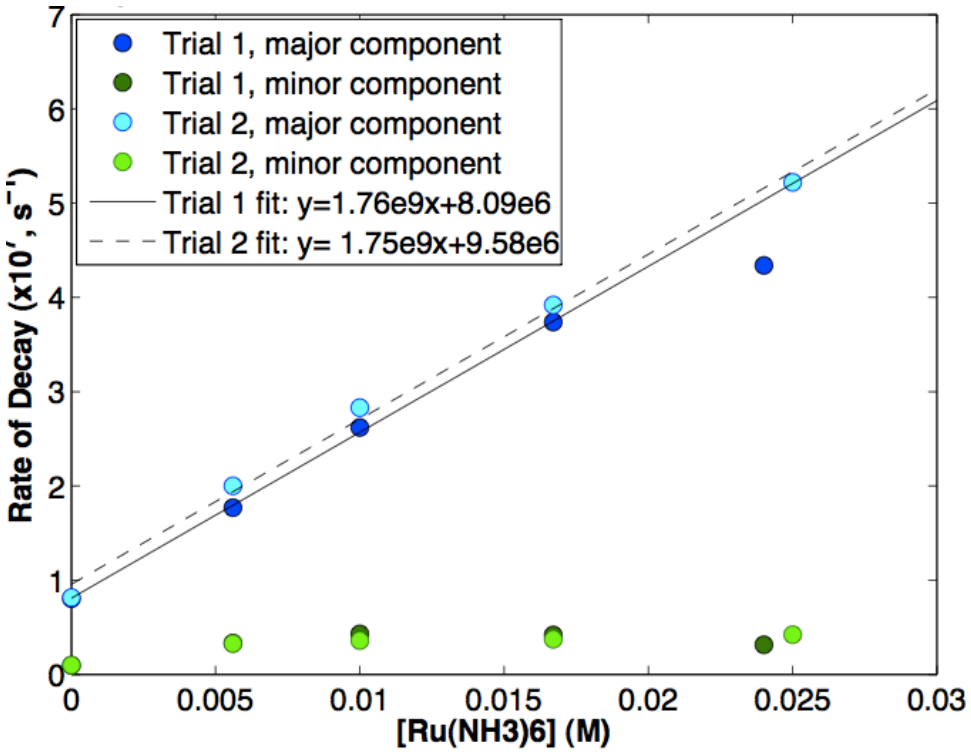

Figure A.12. ET quenching of Ru-NOS with $[Ru^{III}(NH_3)_6]^{3+}$.

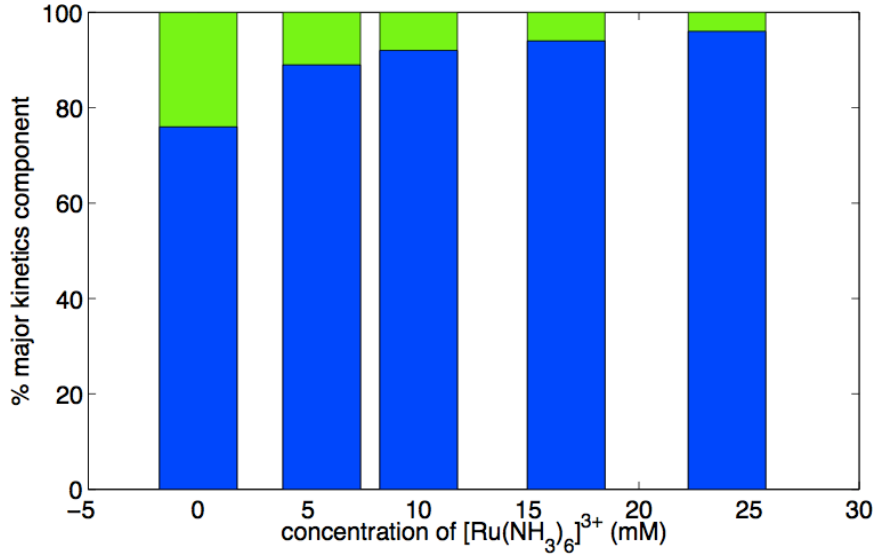

Figure A.13. Relative amplitudes of the major (blue) and minor (green) luminescence decay components for Ru-NOS.

A.2.3. Transient Absorption

As described for Ru-P450, both the Ru photosensitizer and NOS heme have strong electronic absorbance in the 390-440 nm region: NOS Soret ε(λ_{max}: 400 nm) = 79,000 $M^{-1}cm^{-1}$;[9] $[Ru(bpy)_2(Aphen)]^{2+}$ ε(λ_{max}: 450 nm) = 16,600 $M^{-1}cm^{-1}$.[11] The shapes and positions of these electronic transitions are sensitive to metal oxidation state and environment; each species has a distinct absorption profile. By monitoring transient absorption (TA) at multiple wavelengths (390-440 nm) over time, we can identify the formation and decay of ET intermediates following laser excitation.

TA data for flash-quench of Ru-NOS is shown in **Figure A.14**. As described in Chapters 2, 3 and 5, the initial transient absorption feature (10 ns) is a bleach (ΔOD < 0) at all wavelengths examined, with maximum ΔOD at 440 nm. Based on control studies of free photosensitizer, this feature is attributed to the photosensitizer excited state (*Ru^{II}-NOS). This feature decays by ET quenching to form the oxidized, Ru^{III}-NOS species (~100 ns) that is characterized by a similar, bleached absorption profile. TA at 440 nm recovers to baseline within 20 μs. However, TA at 400 nm (λ_{max} of the NOS Soret) remains bleached up to two orders of magnitude longer (2 ms). This is indicative of heme oxidation.

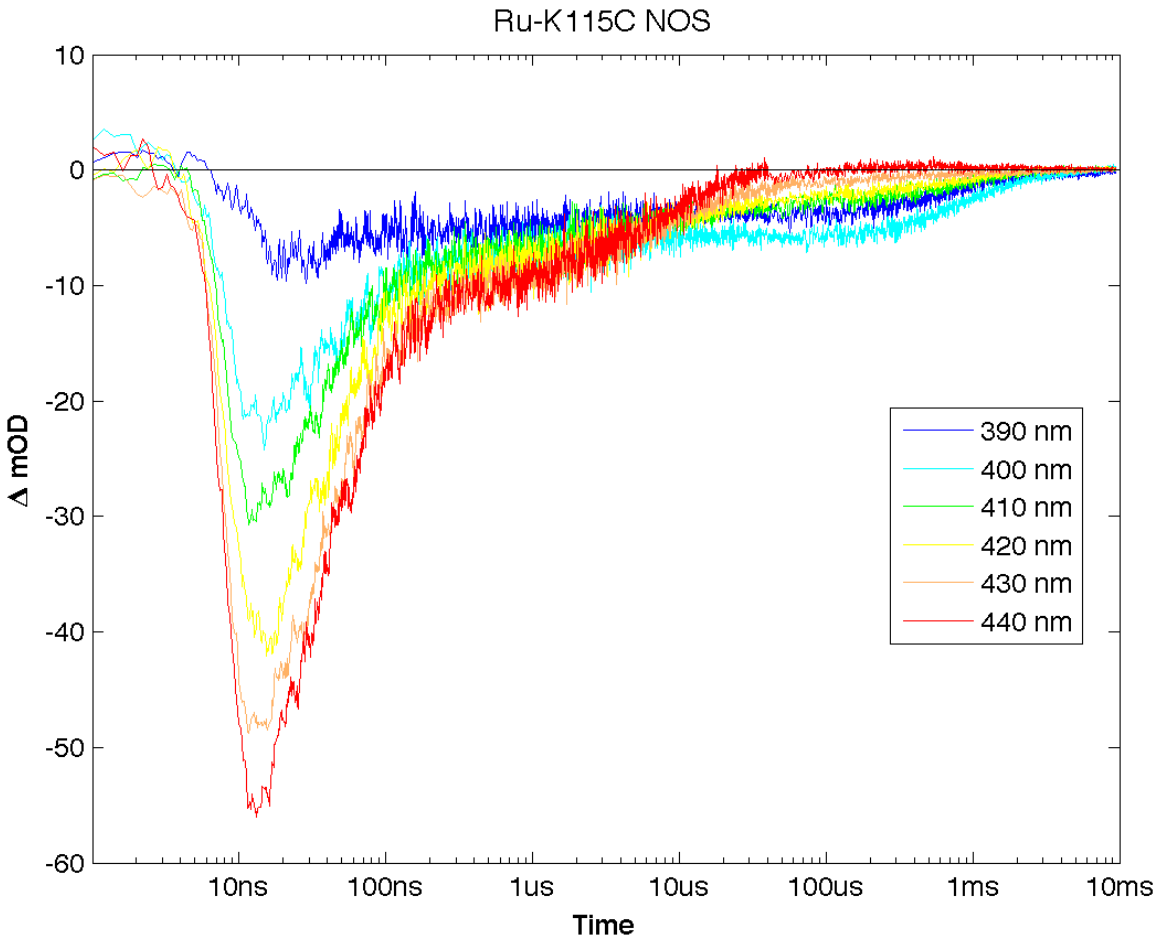

Figure A.14. Transient absorption data at six wavelengths for flash-quenched Ru-NOS.

In order to determine the number of kinetics components associated with Ru-NOS kinetics, and therefore, the number of species, we have subjected TA data at six wavelengths to truncated generalized singular value decomposition analysis (tgSVD) (Regularization Tools, Per Christian Hansen,[12] see sample script in Appendix D). The plot of the tgSVD shows the magnitude (y-axis) of the contribution of each rate constant *k* (x-axis) to the overall fitting of the transient absorption data. Grouping of the rate constants into three clusters indicates that as many as three distinct kinetic phases contribute to the recovery of TA signals to baseline. This is different from analysis of Ru-P450 TA data, in which 5 kinetics phases were identified.

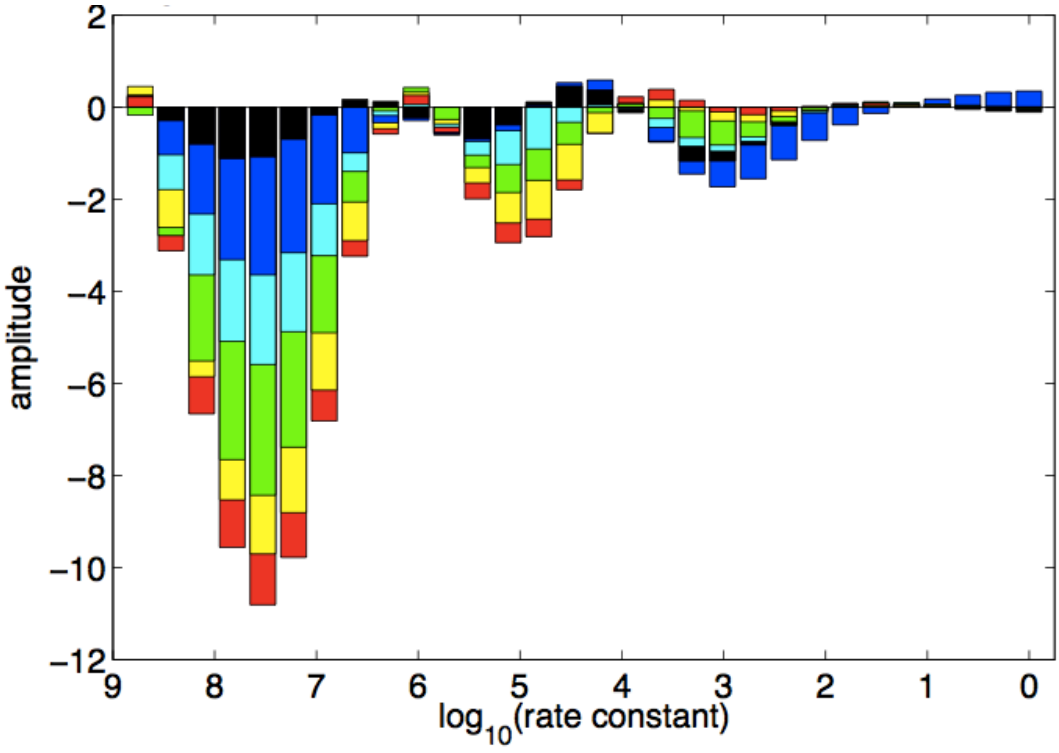

Figure A.15. tgSVD of TA data for flash-quench of Ru-NOS. Red: 440 nm; yellow: 430 nm, green: 420 nm; cyan: 410 nm; blue: 400 nm; black: 390 nm.

We have used the position of each grouping in the tgSVD analysis as an initial guess for multiexponential fitting. Starting with these rate constants, we have performed a global least-squares fitting of the TA data recorded at six wavelengths (390, 400, 410, 420, 430, 440 nm), to a sum of three exponentials with amplitude coefficients $\rho_{1\text{-}3}$ and observed rate constants $\gamma_{1\text{-}3}$ (Equation A.1, **Table A.3**) (see a sample fitting script in Appendix D).

$$TA(\lambda_n) = \rho_{n1}\exp(\gamma_1 t) + \rho_{n2}\exp(\gamma_2 t) + \rho_{n3}\exp(\gamma_3 t) \qquad \text{A.1}$$

Table A.3. Rate constants extracted from global fitting of TA data.

	γ_1	γ_2	γ_3
Rate (s^{-1})	2.2×10^7	1.5×10^5	9.9×10^2
τ (s)	45 ns	7 μs	1 ms

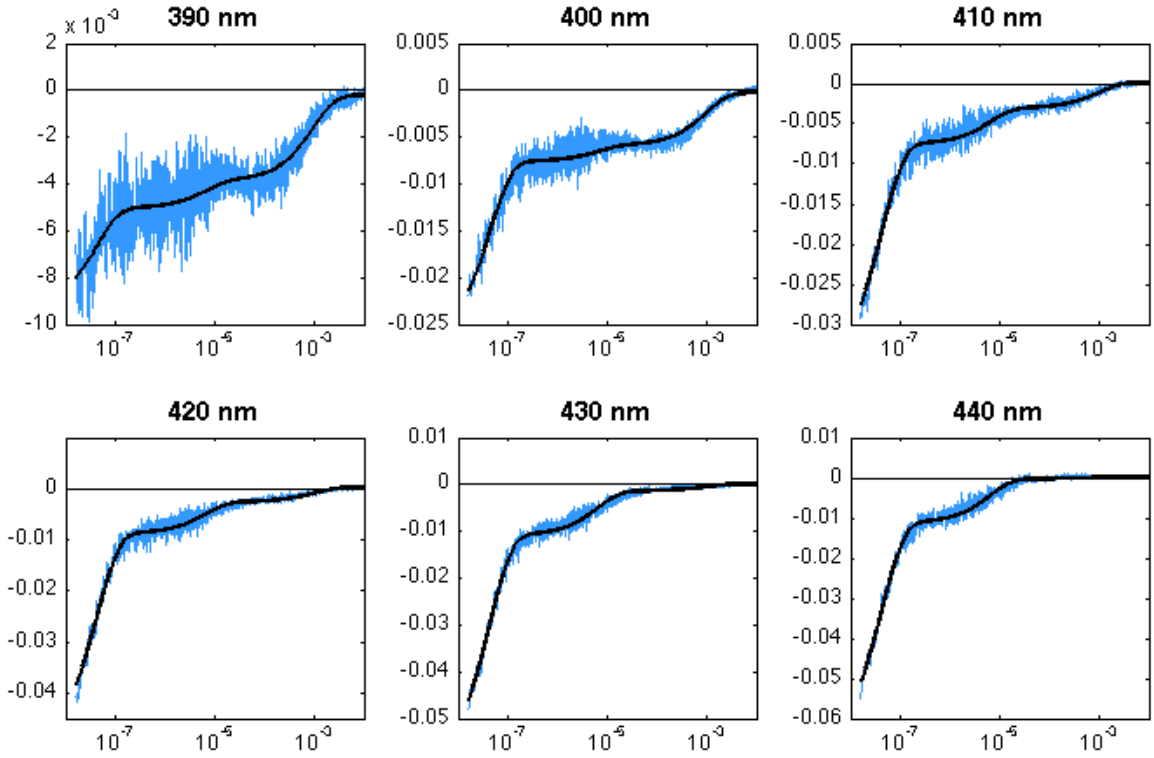

Figure A.16. Global fitting of TA data at six wavelengths.

We can compare the transient features for flash-quenched Ru-NOS to those observed for Ru-P450. In the latter case (see Chapter 2), bleaching of Soret wavelengths on the microsecond-to-millisecond timescale was attributed to formation of porphyrin radical species. These transient intermediates converted to high-valent compound II, which was characterized by a red-shifting of the Soret band. The transient species for flash-quenched Ru-NOS that appears from 10 μs – 2 ms is characterized by bleaching of the NOS Soret (400 nm). This is consistent with formation of the porphyrin radical. No additional intermediates were observed.

A.3. Discussion

Conjugation of $[Ru(bpy)_2(Aphen)]^{2+}$ at non-native cysteine115 generates a Ru-NOS conjugate with a Ru-Fe distance of 25 Å; this is very similar to the analogous

distance in Ru-P450 conjugates. Interestingly, there is also an intervening tryptophan (residue 243) between the photosensitizer and heme. This residue may play a role in facilitating oxidative ET in Ru-NOS, as observed for Ru-P450 (see Chapters 3 and 4). Site directed mutagenesis to modify this residue would help elucidate whether transient oxidation of tryptophan243 facilitates ET over the 25-Å distance.

The biexponential luminescence decay of Ru-NOS indicates the presence of two photosensitizer conformations that do not exchange on the timescale of the luminescence decay. The relative ratio of major and minor decay components (τ_A and τ_B, respectively) is not affected by Ru-NOS concentration, nor by the ionic strength of the buffer. This suggests that the two conformations are not a result of monomer-dimer equilibrium. τ_A is significantly shorter (150 ns vs. 1100 ns), and its decay rate is more affected by ionic strength and quencher concentration than is τ_B. We suggest that the major component arises from a conformation in which the photosensitizer is more solvent exposed, while the minor component is attributed to a conformation in which the photosensitizer is nestled against the protein framework, possibly through hydrophobic contacts.

ET quenching of the Ru^{II}-NOS excited state with $[Ru^{III}(NH_3)_6]^{3+}$ generates a Ru^{III}-NOS species within 100 ns, which in turn oxidizes the NOS active site (**Figure A.17**). We can compare the transient features for flash-quenched Ru-NOS to those observed for Ru-P450. In the latter case (see Chapter 2), bleaching of Soret wavelengths on the microsecond-to-millisecond timescale was attributed to formation of porphyrin radical species. These transient intermediates converted to high-valent compound II, which was characterized by a red-shifting of the Soret band. The transient species for flash-quenched Ru-NOS that appears from 10 μs – 2 ms is characterized by bleaching of the NOS Soret (400 nm). Thus, we tentatively

assign this species as a porphyrin radical cation. No additional intermediates were observed for Ru-NOS.

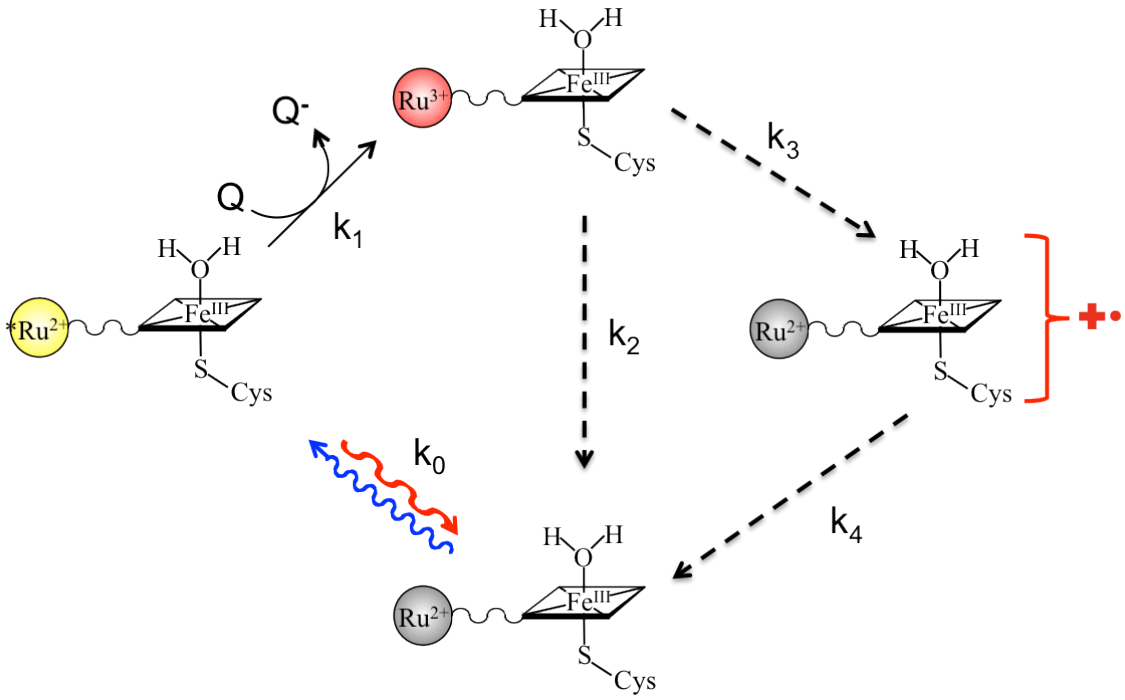

Figure A.17. Scheme for photochemical oxidation of the NOS heme.

A.4. Conclusion

We have developed Ru-NOS conjugates for photo-triggered ET oxidation of the NOS active site. Transient absorption data indicate rapid oxidation of the NOS heme, with a rate constant of (25 μs). We suggest that this proceeds via formation of the porphyrin radical cation, with no evidence of CII formation. Additional investigations, including pH dependence, are necessary to further characterize this transient species.

A.5. Acknowledgments

I would like to thank Dr. Charlotte Whited for NOS insights and expression protocols, and Dr. Gretchen Keller for crystallization of NOS, and for Team Haem Team.

A.6. Materials and Methods

Plasmid for the triple mutant C227S/C269S/K115C NOS with a 6-histidine tag in the pACYCDuet-1 vector (chloramphenicol resistance) was provided by Dr. Charlotte Whited.

Expression Protocols

Plasmid was transformed into BL21DE3 cells (see Appendix B). Overnight cultures of Luria Bertani broth (LB) (25 mL) containing 34 μg/mL chloramphenicol and a single *E. coli* colony (transformed with the mutant plasmid of interest) were incubated at 37 °C overnight, shaking at 180-200 rpm. Induction cultures of LB (3 x 2L) containing 34 μg/mL chloramphenicol were inoculated with the overnight culture and incubated at 37 °C until reaching an optical density of ~1 at 600 nm (~3 hours). Cultures are induced by addition of 1 mM IPTG , and 0.5 mM α-aminolevulenic acid (a heme precursor) and 1 mM $FeCl_3$ is added (values refer to final concentrations in the induction flask). After 24 hours of expression, cells were harvested by centrifugation (5000 rpm, 10 min), and cell pellets are stored at -80 °C until needed.

Extraction and purification

Cell pellets were resuspended in cold Resuspension Buffer (50 mM HEPES pH 7.5, 500 mM sodium chloride, 5 mM imidazole). A small spatula tip each of two

protease inhibitors (benzamidine hydrochloride and Pefabloc SC) were added, and cells were lysed by five cycles of probe-tip sonication (2s on, 2s off, repeat for 2 minutes), cooled by an ice-water bath. Centrifugation (16,000 rpm, 1 hr, 8 °C) pelleted cellular debris, the supernatant was filtered through 0.22 μM filters and loaded onto a HiPrep HisTrap Ni FPLC column (GE Healthcare) equilibrated with Wash Buffer (50 mM HEPES pH 7.5, 500 mM sodium chloride, 10 mM imidazole). After thorough washing with Wash Buffer, protein was eluted with Elution Buffer (300 mM imidazole in Wash Buffer), and the colored (red/orange) fractions are collected.

100 μL of thrombin was added, and the solution was gently agitated at 4 °C overnight to cleave the 6-histidine tag. Following cleavage, the enzyme sample was concentrated using 30 kDa centrifugal filters and subjected to gel filtration on a Superdex 200 FPLC column equilibrated with 50 mM Tris, 150 mM sodium chloride, pH 7.5. Samples were buffer exchanged into 20 mM Tris, pH 7.5 with 20 mM dithiothreitol to reduce intermolecular disulfide bonds. Samples were characterized by UV-vis absorption (A_{420}/A_{280}), SDS-PAGE, and mass spectrometry. Protein not intended for immediate use was flash-frozen in liquid nitrogen (with 40% glycerol added to solution as cryoprotectant) and stored at -80°C.

Ru-NOS conjugation and purification

Photosensitizer synthesis and Ru-enzyme conjugation protocols are described in Appendix B. Ruthenium-labeled and unlabeled NOS were separated by FPLC using a HiTrap Q (GE Healthcare). FPLC Buffers A (column equilibration) and B (elution) were 20 mM Tris, pH 8, and 20 mM Tris, 500 mM sodium chloride, pH 8, respectively. After loading the Ru-NOS sample, the column was washed (3

ml/min) with buffer A until absorbance returned to baseline. The gradient was ramped to 25% (5 min), followed by a slow gradient 25-70% Buffer B over 60 min.

Laser sample preparation, and instrument and data acquisition details for transient luminescence and absorption details are described in Appendix B.

A.7. References

(1) Alderton, W. K.; Cooper, C. E.; Knowles, R. G. Nitric Oxide Synthases: Structure, Function, and Inhibition. *Biochem. J.* **2001**, *357*, 593–615.

(2) Crane, B. R.; Sudhamsu, J.; Patel, B. A. Bacterial Nitric Oxide Synthases. *Annu. Rev. Biochem.* **2010**, *79*, 445–470.

(3) Stuehr, D. J.; Santolini, J.; Wang, Z. Q.; Wei, C. C.; Adak, S. Update on Mechanism and Catalytic Regulation in the NO Synthases. *J. Biol. Chem.* **2004**, *279*, 36167–36170.

(4) Bird, L. E.; Ren, J. S.; Zhang, J. C.; Foxwell, N.; Hawkins, A. R.; Charles, I. G.; Stammers, D. K. Crystal Structure of SANOS, a Bacterial Nitric Oxide Synthase Oxygenase Protein from Staphylococcus Aureus. *Structure* **2002**, *10*, 1687–1696.

(5) Pant, K.; Bilwes, A. M.; Adak, S.; Stuehr, D. J.; Crane, B. R. Structure of a Nitric Oxide Synthase Heme Protein from Bacillus Subtilis. *Biochemistry* **2002**, *41*, 11071–11079.

(6) Gusarov, I.; Starodubtseva, M.; Wang, Z.-Q.; McQuade, L.; Lippard, S. J.; Stuehr, D. J.; Nudler, E. Bacterial Nitric-Oxide Synthases Operate without a Dedicated Redox Partner. *J. Biol. Chem.* **2008**, *283*, 13140–13147.

(7) Zhu, Y.; Silverman, R. B. Revisiting Heme Mechanisms. A Perspective on the Mechanisms of Nitric Oxide Synthase (NOS), Heme Oxygenase (HO), and Cytochrome P450s (CYP450s). *Biochemistry* **2008**, *47*, 2231–2243.

(8) Clague, M. J.; Wishnok, J. S.; Marletta, M. A. Formation of N-Delta-Cyanoornithine from N-G-Hydroxy-L-Arginine and Hydrogen Peroxide by Neuronal Nitric Oxide Synthase: Implications for Mechanism. *Biochemistry* **1997**, *36*, 14465–14473.

(9) Whited, C. A. Tuning Nitric Oxide Synthase: Investigating the Thiolate "Push" and NO Release, California Institute of Technology: Pasadena, California, **2011**.

(10) Keller, G. E. Phototriggering Nitric Oxide Synthase from Geobacillus Stearothermophilus, California Institute of Technology: Pasadena, California, **2013**.

(11) Castellano, F. N.; Dattelbaum, J. D.; Lakowicz, J. R. Long-Lifetime Ru(II) Complexes as Labeling Reagents for Sulfhydryl Groups. *Anal. Biochem.* **1998**, *255*, 165–170.

(12) Hansen, P. C. Regularization Tools: A Matlab Package for Analysis and Solution of Discrete Ill-Posed Problems. *Numer. Algorithms* **1994**, *6*, 1–35.